

# Supporting Information

Zhou et al. 10.1073/pnas.1505800112

## SI Text

**Electric Modeling of Graphene Microphone.** The electrically conducting vibrating graphene diaphragm forms a variable capacitor with the fixed electrodes, with capacitance

$$C = \frac{\epsilon A}{x}, \quad [\text{S1}]$$

where  $\epsilon$  is vacuum permittivity,  $A$  is the area of the graphene membrane, and  $x$  is the distance from one of the electrodes to the graphene membrane. When the diaphragm is dc biased at  $V \sim 50$  V, charge is induced on the electrodes, described by  $Q = CV$ . The vibration of the diaphragm varies the system capacitance and induces charge variation on the electrodes, creating a current

$$i = \frac{dQ}{dt} = \frac{d(CV)}{dt} = V \frac{d(\epsilon A/x)}{dt} = -V \epsilon A \frac{1}{x^2} \frac{dx}{dt} = -\frac{V \epsilon A}{x^2} u, \quad [\text{S2}]$$

where  $u$  is the velocity of the membrane relative to the electrode. Hence, the graphene microphone can be modeled as a current source with an infinitely large internal resistance, where the current encodes the sound wave. In the thin membrane limit where the graphene diaphragm vibrates together with air,  $u$  equals the local velocity field of the air, whose amplitude  $U$  is (21)

$$U = \frac{p}{Z}, \quad [\text{S3}]$$

where  $p$  is the sound pressure level (SPL) and  $Z = 400 \text{ N}\cdot\text{s}\cdot\text{m}^{-3}$  is the acoustic impedance of air. Thus, the amplitude of the microphone current source is directly proportional to the loudness of the sound, and independent of sound frequency. Using Eqs. S2 and S3 with  $V = 50$  V,  $A = 25 \text{ mm}^2$ , and  $x = 150 \text{ }\mu\text{m}$ , we find that at 40 dB SPL (approximately soft conversation at 1 m), the current amplitude is 2 pA. This level of current can only be reliably measured with careful design of the signal conditioning circuit.

### High-Frequency Circuit Design for Extracting Microphone Signals.

Conventionally (12) (Fig. 1D), a large resistor  $R$  (e.g., 10 M $\Omega$ ) is used to convert the current into a voltage, and the voltage signal is subsequently amplified by an operational amplifier. However, this circuit presents difficulties at higher frequencies because of parasitic capacitance in the transmission lines. As can be seen in the equivalent circuit model Fig. 1D, *Right*, at higher frequencies the parasitic capacitance exhibits a small impedance and reduces the voltage drop across  $R$ . For example, even 1 pF of parasitic capacitance (equivalent to  $\sim 1$  cm length of RG-58 coaxial cable) limits the circuit's response to  $1/2 \pi RC = 16$  kHz; this may be acceptable for acoustic microphone circuits, but precludes detecting ultrasonic signals from 20 kHz into the megahertz range.

To circumvent the limitations of the conventional circuit of Fig. 1D, we adopt a current sensing circuit similar to one used in fast photodiode signal detection (14) (Fig. 1E). The operational amplifier is here configured so that the microphone electrode is directly connected to virtual ground. As a result, the parasitic capacitance in the equivalent circuit is effectively shorted, yielding  $i_{\text{out}} = i_{\text{mic}}$  and  $v_{\text{out}} = R \cdot i_{\text{out}} = R \cdot i_{\text{mic}}$ . The output voltage is now directly proportional to the microphone vibration and not affected by parasitic capacitance. The circuitry of Fig. 1E is used to characterize the microphone for this report.

**Microphone Operation Mechanism.** A traditional microphone measures the voltage variation of the vibrating membrane. The operation is shown in the following equation. Basically, because the membrane is connected to a very large resistor, the charge  $Q$  remains almost constant during operation. Gauss's law gives us the voltage drop between two plates with charge  $Q$ :

$$V = Ed = \frac{Q(d_0 + A \sin(\omega t))}{S \epsilon},$$

where  $Q$  is the charge on membrane,  $d_0$  is the distance between membrane and the electrode at balanced position,  $S$  is the area of the membrane,  $A \sin(\omega t)$  is the membrane vibration displacement with amplitude  $A$ , and  $\epsilon$  is vacuum permittivity. We see that if we measure the voltage response, the AC portion is proportional to  $A$ , the amplitude of vibration displacement.

In this case an overdamped system does not generate flat-band response. If we model the system as a harmonic oscillator, the equation is:

$$m\ddot{x} + \zeta\dot{x} + kx = F = SP \sin(\omega t),$$

where  $m$  is the membrane mass,  $\zeta$  is the damping coefficient,  $k$  is the spring constant, and  $F$  is the driving force applied on the diaphragm, which equals the sound pressure  $SP \sin(\omega t)$ . The solution of the vibration amplitude is

$$A = |x| = \frac{SP}{|\zeta\omega - ik + i\omega^2 m|}.$$

If the system is overdamped, the damping term  $\zeta\omega$  will dominate over other terms, therefore resulting in  $A \sim \omega^{-1}$ , which means that the measured voltage signal will also reduce as the frequency goes up; this is the case for traditional microphone where a relatively high tension membrane is desired, so that the spring constant term  $k$  can dominate to have flat-band response.

As we noted previously, our microphone uses the current sensing mechanism to support working in the high-frequency region. As shown in the following equation, our circuit measures vibration velocity instead of displacement.

The membrane is held at voltage  $V$ , so the amount of charge on the membrane is actually changing, generating a current where we extract the vibration information. The charge on the membrane or on the fixed electrode can be easily computed using a parallel plate capacitor:

$$Q = CV = \epsilon SV/d = \epsilon SV/d_0 + A \sin(\omega t).$$

The vibration amplitude is usually much smaller than the distance between the membrane and the electrode, so at  $A \ll d_0$  we can Taylor expand the expression to the first order:

$$Q \approx \frac{\epsilon SV}{d_0} \left[ 1 - \frac{A}{d_0} \sin(\omega t) \right].$$

So the time variation of charge is the measured current:

$$i = dQ/dt = -\epsilon SV A \omega / d_0^2 \cos(\omega t).$$

We see here that the amplitude of the measured current is proportional to  $A\omega$ . Now we return to the motion equation and find

$$|i| \propto A\omega = \frac{SP}{|\zeta - ik/\omega + i\omega m|}$$

Therefore, an overdamped system, where the damping term  $\zeta$  dominates other terms, results in a constant current amplitude, i.e., a flat-band frequency response.

**Construction of Graphene Microphone.** A 1-cm<sup>2</sup> piece of 25- $\mu$ m-thick nickel foil is first electrochemically polished (22, 23), cleaned by deionized water, and loaded into a 25-mm-diameter quartz tube furnace (Fig. S3A). After hydrogen annealing, the graphene layers are grown by chemical vapor deposition process at 1050 °C with 50 sccm methane and 50 sccm hydrogen coflow. The growth chamber pressure is controlled at 1 Torr. The growth lasts 15 min, and the methane flow rate is increased to 200 sccm for the last 2 min to improve the stitching between graphene grains (24). The foil is then quickly cooled down to quench the graphene growth (25) (Fig. S3B). After unloading, a layer of poly (methyl methacrylate) (PMMA) is spin-coated on top of the nickel foil (Fig. S3C), and the graphene on the other side of the foil is etched away using an oxygen plasma (1 min at 100 W; Fig. S3D). A circular aperture of 8 mm diameter is created with a disk cutter on a sticky Kapton tape serving as a supporting frame. The supporting frame is then attached to the PMMA layer on the nickel foil (Fig. S3E). The nickel foil is subsequently etched away in 0.1 g/mL sodium persulfate solution (Fig. S3F). Compared with the iron chloride solution used previously (11, 25), here the etch rate is much lower (typically overnight etching is required to remove the 25- $\mu$ m-thick nickel), but the resulting graphene diaphragm is very clean and free of amorphous carbon. The exposed (not covered by the supporting frame) area of the PMMA layer is then dissolved in acetone, and the graphene layer supported by the frame is cleaned twice with isopropanol and dried in air (Fig. S3G). The PMMA between the supporting frame and graphene serves as a buffer material and improves the yield to ~100% [the PMMA-free process (11) has a typical yield of ~30%]. The membrane is measured by light transmission (11) to be ~20 nm thick, or 60 monolayers of graphene. A 25- $\mu$ m diameter gold wire is attached to the edge of the graphene membrane for electrical contact (Fig. S3H). Finally, spacers of ~150  $\mu$ m thick are attached to both sides of the frame, followed by perforated electrodes made from silicon wafers using deep reactive ion etch. The rigid electrodes are also wired with gold wires attached by silver paste (Fig. S3I). The surfaces of the electrodes facing the graphene membrane are coated with conductive metal layers (20 nm sputtered gold) to allow ohmic contact between the gold wire and the electrodes. This gold coating is essential for eliminating any contact barrier that could block the current flow during microphone operation, because the voltage variation on the membrane is very small. We note that for loudspeaker applications, this metal coating is not necessary because large voltages are there applied.

Optionally, a waveguide or a Helmholtz acoustic cavity can be attached to the microphone assembly, modifying the FR of the microphone in the low-frequency region by altering the damping or creating/eliminating interference (21). Without these modifications, the sound pressure forces at the front and the backside of the diaphragm tend to cancel at low frequencies, resulting in diminished response.

**Measurement of the Membrane Tension.** A setup similar to the one used to measure graphene resonators (16, 26) are used to measure the resonate frequency of the graphene diaphragm in vacuum. We have loaded the microphone into the optical chamber, applying a small AC voltage (1 V) upon the 50-V DC bias between the electrodes and graphene membrane as a source of actuation force. The vibration of the graphene membrane versus frequency

is then measured optically by laser interference. The frequency sweep data collected by the network analyzer is presented here.

As we can see, the membrane has a resonating frequency at 3.175 kHz. Therefore, we can extract the effective spring constant of the membrane to be

$$k = m(2\pi f_0)^2 \\ = 1.7 \times 10^4 \text{ N/m}^3 \text{ (per area effective spring constant).}$$

We can also deduce the stress on the membrane.

The resonating frequency of a circular membrane is (27):

$$f_0 = \frac{4.808}{2\pi D} \sqrt{\frac{\sigma}{\rho}},$$

where  $D = 7$  mm is the diameter,  $t = 20$  nm is the thickness,  $\rho = 4.4 \times 10^{-5}$  kg/m<sup>2</sup> is the mass density, and  $\sigma$  is the stress. The stress of the membrane is therefore

$$\sigma = \left( \frac{2\pi D f_0}{4.808} \right)^2 \rho t = 1.85 \text{ MPa.}$$

**Detailed Frequency Response Measurement Procedure.** To determine the frequency response of the graphene microphone, we first sweep the frequency on a commercial loudspeaker and measure the response of a commercial microphone to obtain the frequency response  $FR_1(f)$  of the measurement system, which contains responses of individual components:

$$FR_1(f) = FR_{CM}(f) + FR_{CL}(f) + FR_C(f) + FR_A(f), \quad \text{[S4]}$$

where  $FR_{CM}$  and  $FR_{CL}$  represents the FR of the commercial microphone and commercial loudspeaker, respectively,  $FR_C$  is the FR of the coupling between loudspeaker and microphone, and  $FR_A$  is the FR of the driving/amplification circuits for the loudspeaker/microphone. The responses are added because they are measured on a decibel scale (logarithm of amplitude). Next the commercial microphone is replaced with the graphene microphone and the measurement is repeated:

$$FR_2(f) = FR_{GM}(f) + FR_{CL}(f) + FR_C(f) + FR_A(f) \quad \text{[S5]}$$

where  $FR_{GM}(f)$  is the response of the graphene microphone. From Eqs. S4 and S5 we find

$$FR_{GM}(f) - FR_{CM}(f) = FR_2(f) - FR_1(f). \quad \text{[S6]}$$

The FR of the graphene microphone referenced to the commercial microphone can therefore be acquired by taking the difference between the two measurements. This differential measurement method eliminates the responses of the loudspeaker, coupling, and driving/amplification circuits. Commercial microphones typically have a relatively flat frequency response  $FR_{CM}(f)$  within their operating range, compared with loudspeakers  $FR_{CL}(f)$  and coupling  $FR_C(f)$ , and therefore this measurement provides a reasonable representation of the graphene microphone  $FR_{GM}(f)$ .

As described in the main text, acoustic wave diffraction at longer wave lengths causes interference and reduced responses. To determine the intrinsic response of the graphene diaphragm unburdened by diffraction, we choose to (i) use acoustic cavity to block the backside of the graphene microphone; and (ii) closely place an earbud sized speaker (Sennheiser CX-870) ~3 mm away from the microphones (both commercial and graphene) to reduce diffraction. As shown in Fig. 2B, the near-field coupling largely eliminates low-frequency interference and the graphene

microphone now exhibits an intrinsic flat (<10 dB variation) frequency response across the whole audible region.

Due to the small areal mass density of the thin graphene diaphragm, the graphene microphone is expected to be responsive to frequencies well beyond the human hearing limit. However, measuring the frequency response in the ultrasonic region presents difficulties, mainly due to the lack of wideband reference microphones or loudspeakers in this region. As mentioned, piezoelectric ultrasonic transducers readily operate in the megahertz region, but only at their resonance frequency. We therefore use a wideband electrostatic graphene loudspeaker as the sonic transmitter and the electrostatic graphene microphone as the receiver. The combined system frequency response is then

$$FR_S(f) = FR_{GM}(f) + FR_{GL}(f) + FR_C(f) = 2FR_{GM}(f) + FR_C(f), \quad [S7]$$

where it has been assumed that the graphene microphone and loudspeaker have the same FR behavior. Because the coupling term  $FR_C(f)$  cannot in this case be directly eliminated, we design an experiment to approximate its contribution.

Fig. S6 illustrates the measured frequency response of the loudspeaker–microphone pair (a network analyzer, model HP3577A, is used for the measurement because the frequencies exceed the limits of a conventional computer sound card). The response appears to be relatively flat from ~100 Hz to ~0.5 MHz. To distinguish the contribution from the coupling term  $FR_C(f)$ , the distance between the loudspeaker–microphone pair is varied to change  $FR_C(f)$ . Two measurements are shown in Fig. S6 for the pair, 4 cm apart and 10 cm apart. The coupling mainly affects the behavior in low-frequency region (<2 kHz). In this region, the coupling of the 10-cm pair becomes increasingly weak as frequency drops compared with the 4-cm pair, which can be attributed to sound wave interference as mentioned previously. In the high-frequency region (>2 kHz), the 10-cm curve has the same form as the 4-cm curve with total intensity shifted down by ~8 dB (see the guide to the eyes, distance between the two lines are 7.2 dB). This reduction of the total intensity is simply attributed to the inverse-square law required by energy conservation [8 dB = 6.3 in energy ratio  $\simeq (10 \text{ cm}/4 \text{ cm})^2$ ]. We therefore assume a relatively flat  $FR_C(f)$  in this region, and from Eq. S7,  $FR_S(f) = 2FR_{GM}(f)$ . The measured  $FR_S(f)$  varies less than 20 dB until ~0.5 MHz, indicating less than 10 dB variation of the graphene microphone alone. To translate this data to the ones presented in Fig. 2C, we take the response curve of 4 cm apart above 2 kHz, compress the curve by a factor of 2 ( $FR_S(f) = 2FR_{GM}(f)$ ), and do a 4-point average noise reduction. The more noisy data at higher frequency is probably due to transmitter–receiver positioning-caused interference, because we found the noise over the baseline is highly sensitive to the positioning.

#### Sawtooth-Modulated Sine Wave Transmission by Piezoelectric Transducer.

Sawtooth-modulated sine wave shown in Fig. 3B is analyzed to give the following power spectrum. As shown in Fig. S7, the spectrum spreads out from a delta-function-like peak. A typical piezoelectric transducer has a quality factor of  $\sim 10^4$ , where  $Q$  can be estimated from its operating frequency and response time. The transducer therefore has a bandwidth of  $\sim 30$  Hz, which is too narrow to pass through all of the frequency components from sawtooth-modulated sine wave.

**Position Detection Using Interference Method.** The EM antenna is intrinsic. As shown in Fig. S4, the transmitter and receiver are normally encapsulated in an acoustic cavity/Faraday cage. When the shielding is incomplete (e.g., not completely enclosed Faraday cage), the electrical feeding wires serves as EM antenna to transmit and receive EM waves. Because EM waves travel orders of magnitude faster than acoustic waves, the exact shape and location of EM antenna have very small effect on the distance measurement.

As seen in Fig. 3C, when a frequency sweep is performed, the interference alternates between constructive and destructive due to the change in the wavelength  $\lambda$ . The condition for constructive interference is

$$\frac{L}{\lambda} = n, \quad [S8]$$

where  $L$  is the distance between the microphone and the loudspeaker,  $\lambda$  is the wavelength of the sound wave, and  $n$  is an integer. The nearest two constructive peaks should obey

$$\frac{L}{\lambda_1} = n \quad \text{and} \quad \frac{L}{\lambda_2} = n + 1. \quad [S9]$$

Using  $\lambda = v/f$ , where  $v$  is the sound velocity and  $f$  is the frequency, we obtain

$$\frac{L}{v}(f_2 - f_1) = 1 \quad \text{or} \quad L = \frac{v}{\Delta f}. \quad [S10]$$

The distance  $L$  simply equals the sound velocity divided by the frequency difference  $\Delta f$  of two nearest constructive interference peak. We place the graphene speaker/microphone pair three different distances apart at 30, 45, and 85 mm. The measured frequency sweep is shown from top to bottom in three groups in Fig. 3C. When the pair is further apart, the signal is weaker, and the frequency difference between two constructive peaks also becomes smaller. By fitting in all of the peaks, we find frequency differences  $\Delta f$  of  $11.28 \pm 0.08$ ,  $7.657 \pm 0.003$ , and  $4.05 \pm 0.07$  kHz, respectively; using a sound velocity of 344 m/s, this corresponds to a measured distance of  $30.49 \pm 0.22$ ,  $44.92 \pm 0.02$ , and  $84.94 \pm 0.84$  mm.

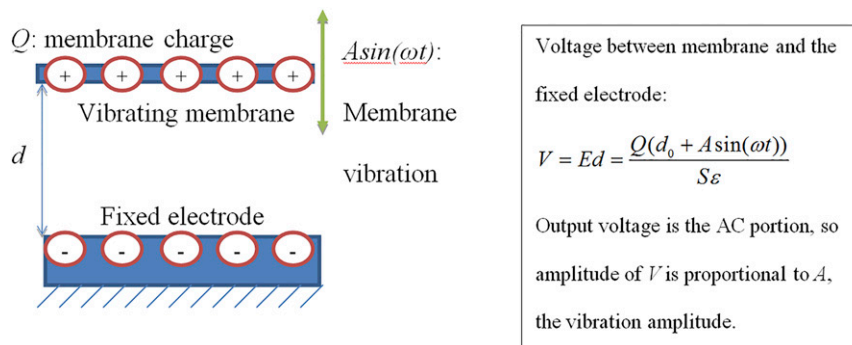


Fig. S1. Operation of traditional condenser microphone, which generate signals proportional to membrane displacement.

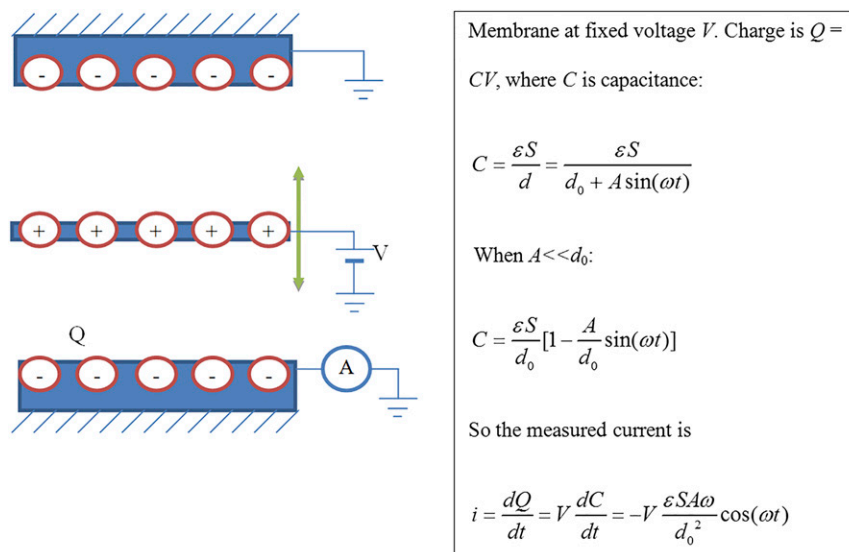


Fig. S2. Operation based on current sensing, signal proportional to membrane velocity.

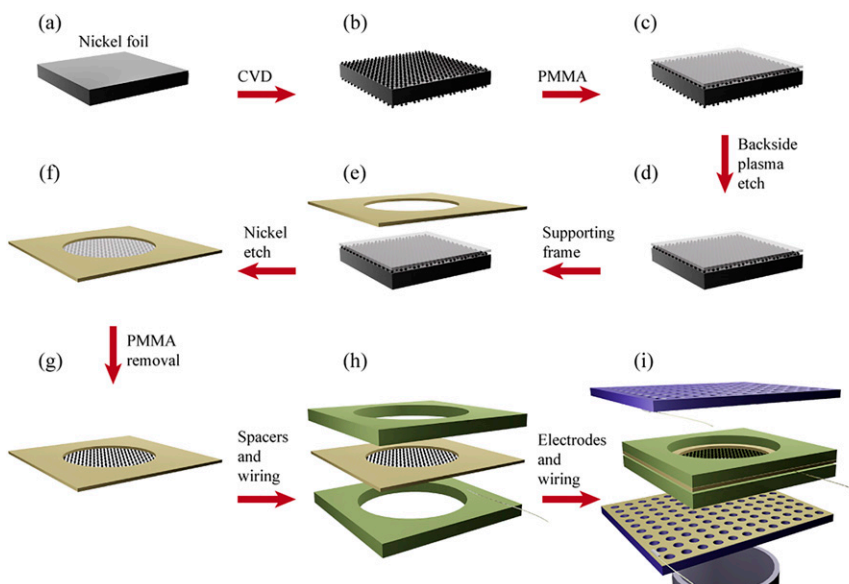
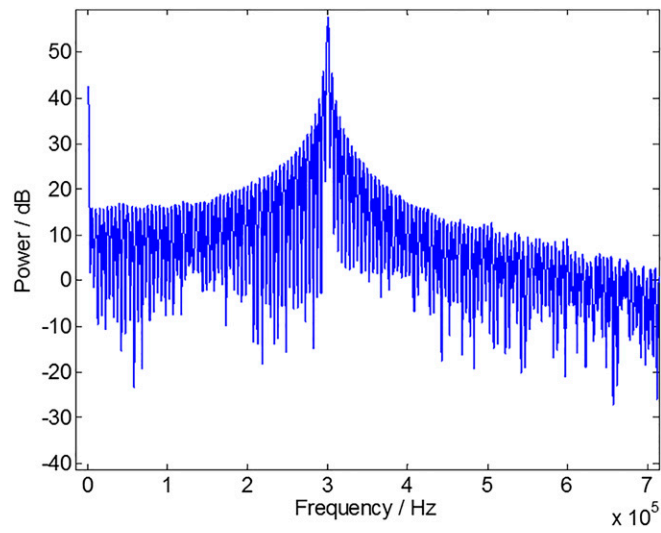


Fig. S3. (A-I) Fabrication process of graphene electrostatic microphone.





**Fig. S7.** The power spectrum of sawtooth-modulated sine wave.

**Audio File S1.** A direct recording (amplitude vs. time) of bat (western pipistrelle or *Parastrellus hesperus*) calls at Del Valle Regional Park, Livermore, CA. The audio file is slowed down 8x to bring the ultrasonic chirps into human audible region.

[Audio File S1](#)